ACS OMEGA

Open Access

http://pubs.acs.org/journal/acsodf

Article

Sustainable Engineered Designs and Manufacturing of Waste Derived Graphenes Reinforced Polypropylene Composite for Automotive Interior Parts

Havva Baskan-Bayrak, Ramisa Yahyapour, Yavuz Emre Yagci, and Burcu Saner Okan*

Cite This: *ACS Omega* 2024, 9, 34530−34543

Read Online

ACCESS | Metrics & More | Article Recommendations | Supporting Information

ABSTRACT: The automotive sector is actively pursuing a lightweighting strategy as a means to urgently decrease greenhouse gas emissions, which are a significant driver of climate change. The development of lightweight composite structures has been identified as crucial for enhancing part performance while mitigating negative environmental impacts and adopting energy-efficient manufacturing methods. This comprehensive study aimed to decrease the main reinforcement content of talc in commercial compounds while integrating graphene derived from waste polypropylene (PP) grown on talc and graphene nanoplatelet obtained from waste tires by upcycling processes into the PP compound. The entire value chain of interior automotive part production, from compound development and scaling up with a high-shear mixer, to injection molding of the part and performance tests, was investigated with a focus on sustainability considerations. The successful integration of 4 wt % micron talc, together with 1 wt % graphene nanoparticles and 1 wt % hybrid additive into the blended HomoPP/CopoPP matrix resulted in a 10% weight reduction compared to the conventional part. Moreover, significant improvements in flexural and tensile strength were observed, with enhancements of 52 and 38%, respectively. The uniform dispersion of additives and improved interfacial adhesion between the PP matrix and additives facilitated efficient stress transfer, contributing to enhanced mechanical properties. Furthermore, a systematic life cycle assessment study demonstrated the positive impact of waste PP incorporation on CO_2 reduction, achieving a remarkable 95% reduction compared to virgin PP. The developed compound also demonstrated favorable processability and flow properties, supporting its potential for mass production. Overall, this study presents a sustainable and effective approach for lightweight automotive interior part production using a synergistically designed PP compound meeting the requirements of the automotive industry.

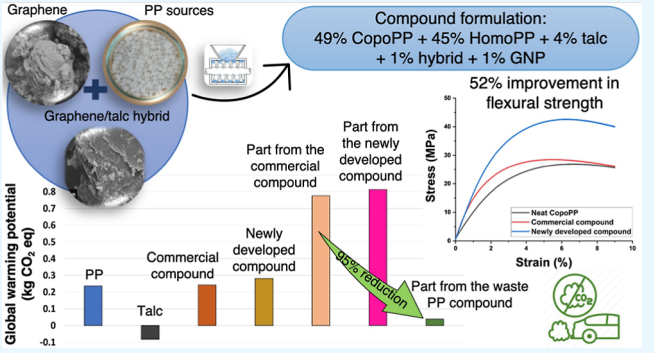

1. INTRODUCTION

Over the past decade, the automotive sector has made pioneering innovations in environmental sustainability which involves optimizing material choices for lightweighting and durability.[1,2] The shift toward advanced materials for lightweight and high-strength characteristics has driven the adoption of polymer composites as alternatives to traditional metal parts, aligning with broader sustainability goals.[3−5] Polypropylene (PP) is extensively employed as a polymer matrix in polymer composites due to its low density and cost, favorable processability, remarkable thermal stability and chemical resistance, and recyclability.[6,7] Additionally, PP shows great compatibility for reinforcement or blending with various polymeric materials or organic/inorganic additives.[8] However, due to its inadequate impact performance and low modulus, the PP matrix is primarily combined with calcium carbonate ($CaCO_3$), clay, silica, or talc to improve its mechanical, thermal, and rheological properties.[9,10] In particular, talc, characterized by its layered structure of magnesium silicate, serves as both a reinforcement and a cost-saving element in PP composites while improving their toughness.[11] The reinforcing effect of talc could be notably observed up to 20 wt % loading.[12,13] Guerrica-Echevarria et al. proved the increased Young's modulus, with nearly a 40% enhancement in modulus observed for each 10% increment in talc content, by using injection-molded PP composites containing 10, 20, and 40% talc.[14] Furthermore, Castillo et al. declared that macrocrystalline talc presence resulted in an 8% higher Young's modulus and 25% greater yield stress compared to microcrystalline talc in the injected-molded PP/talc composites.[15] Talc has also been shown to modify PP

Received: March 17, 2024
Revised: July 10, 2024
Accepted: July 15, 2024
Published: August 3, 2024

composites by reducing the coefficient of linear thermal expansion of PP, thereby enhancing dimensional stability.[16] Additionally, studies have demonstrated the nucleating effect of talc, promoting faster solidification during injection molding.[17] However, the incorporation of talc filler is not without drawbacks. Increased part density is typically observed, potentially impacting weight and application suitability. Furthermore, talc can negatively affect the ductility of the material, limiting its flexibility.[18]

On the other hand, nanoparticles or nanofillers offer a considerably greater surface area and enhanced interfacial adhesion compared to microscale fillers, which makes them the preferred option for boosting the thermal, mechanical, and physical properties of polymer composites. The successful integration of these nanofillers into the polymer matrix greatly depends on their particle size, which plays a pivotal role in maximizing the performance of composites.[19] In this sense, graphene is often referred to as the perfect nanofiller for polymer composites due to its exceptional specific surface area, high thermal conductivity, and mechanical strength.[20,21] El Achaby et al. demonstrated significant improvements in the mechanical performance of PP nanocomposites by incorporating graphene. They reported a 100 and 81% enhancement in tensile strength and Young's modulus, respectively, upon the addition of 3 wt % graphene nanosheets compared to neat PP.[22] Specifically, the addition of graphene nanoparticles (GNP) into PP composites improves conductivity, thermo-mechanical behavior, thermal stability, and crystallinity.[23] For instance, a response surface methodology study by Rocha et al. revealed that incorporating GNP with a high surface area of 750 m^2/g, a volumetric density of 0.2−0.4 g/cm^3, and a particle size less than 2 μm improved the flexural properties and thermal stability of PP composites.[24] In a separate study, Liang et al. incorporated 0.1 to 0.5 wt % of GNP into PP and obtained approximately a 63% enhancement in the flexural modulus specifically at the 0.4 wt % GNP weight ratio.[25] In another study, Patra et al. developed PP nanocomposites by loading 1, 2, and 3 wt % GNP of three lateral sizes (5, 15, and 25 μm), all having a consistent thickness (15 nm) and surface area (50−80 m^2/g), and achieved a 38% increase in flexural strength and a 132% improvement in impact strength with the 3 wt % loading ratio of 25 μm lateral sized-GNP while 86% enhancement in tensile strength with the same loading of 5 μm lateral sized-one.[26] On the other hand, Sutar et al. declared 105 and 16% advancements in tensile and flexural strength, respectively, by the addition of 5 wt % GNP, having a surface area of 120−150 m^2/g and thickness of 6−8 nm, into PP composite.[27]

Furthermore, instead of utilizing virgin GNP produced by conventional graphene synthesis methods such as Hummers' technique, the usage of recycled/upcycled GNP in the PP composites contributes to both improving the mechanical characteristics of the composites and sustainability by reducing the carbon footprint. For instance, Zanjani et al., developed waste tire derived graphene-reinforced PP nanocomposites. The presence of 1 wt % GNP resulted in a 7 °C increase in crystallization onset temperature for the copolymer (Copo-) PP matrix, indicating the nucleation agent effect of GNP, promoting the crystallization of PP during the cooling cycle.[28]

This study aimed to develop a novel, lightweight, and sustainable compound formulation for B-pillar interior automotive parts, offering an alternative to the currently used 15 wt % talc-filled CopoPP compounds. A holistic approach was employed by investigating the entire production chain, from compound development to injection molding and performance validation of the B-pillar interior part through real-case thermal and structural finite element analysis (FEA). During compound development, the focus was on reducing primary reinforcement content and integrating waste-driven, sustainable additives using a high-shear mixing technique. To the best of our knowledge, no previous research has integrated waste resources like waste PP to obtain sustainable reinforcing additives. This approach reduces the need for virgin material, leading to a lower environmental footprint. The tailored formulation not only achieved high mechanical strength and thermal stability but also resulted in a 10% weight reduction compared to the current commercial compound used in part production. Additionally, utilizing waste PP, led to a remarkable 95% reduction in CO_2 emissions. Consequently, the B pillar interior part manufactured using this formulation holds the promise of improved performance and substantial sustainability advantages.

2. EXPERIMENTAL SECTION

2.1. Materials. Micron talc with an average particle diameter of d_{50} = 12 μm and a density of 2.78 gr/cm^3 was supplied from Micron'S Company (Turkey). Iron chloride [$FeCl_3$ (≥97%)] was purchased from Sigma-Aldrich to functionalize the talc surface. Iron-treated micron talc (Fe-micron talc) and upcycled graphene/Fe-micron talc hybrid additive were produced in our lab as described in our previous studies.[29,30] Graphene nanoplatelet (GNP), from the recycling and upcycling of waste tires, was obtained from Nanografen Company (Turkey) with a 9 wt % surface oxygen groups content, a density of 2.11 gr/cm^3, a surface area of 120 m^2/gr, and an average platelet size of 50 nm.[31] XRD, Raman, and SEM characterization results of upcycled graphene/Fe-micron talc hybrid additive and GNP are given in the supplementary document in Figures S1 and S2, respectively. Homopolymer PP (HomoPP, BUPLEN 6331) with a melt flow rate of 12 g/10 min and elastomer-filled copolymer PP (CopoPP, TOTAL PPC712) with a melt flow rate of 25 g/10 min at 230 °C were provided from Basell Company (Turkey) and Ravago Plastics Company (Turkey), respectively. Additionally, as a reference, the commercial CopoPP composite containing 15 wt % talc, with a melt flow rate of 19 g/10 min at 230 °C, was received from Farplas Company (Turkey). Mechanically recycled waste PP, originally unknown source, was provided from Vanden Recycling Company (Turkey) (Figure S3).

2.2. Fabrication of CopoPP Compounds Reinforced with Talc and Waste-Driven GNP. Talc, graphene/talc hybrid, and GNP reinforced CopoPP composites were prepared by a thermokinetic mixer (Dusatec, USA) with a shear rate of 4000 rpm and a temperature of 180 °C. The incorporation of HomoPP into the CopoPP matrix was considered, as well. Table S1 summarizes the composition details of the prepared samples which are labeled according to their respective contents. Subsequently, the resulting compounds were granulated by using a mechanical crusher and molded by an explore injection molding machine (Xplore, Sittard, The Netherlands) into ISO 527-2 tensile and ISO-178 flexural test specimens (Figure S4).

2.3. Injection of B Pillar Interior Part from the Optimized Compound Formulation. In serial production, the B pillar interior part is fabricated from the commercially available 15% talc-reinforced CopoPP compound. Within this

https://doi.org/10.1021/acsomega.4c02596
ACS Omega 2024, 9, 34530−34543

Table 1. Flexural Modulus and Strength of Talc-Reinforced CopoPP Composites

sample	flexural modulus (MPa)	improvement (%)	flexural strength (MPa)	improvement (%)
neat CopoPP	985.0 ± 25.1		26.8 ± 0.1	
CopoPP + 5% talc	1260.0 ± 20.4	27.9	30.8 ± 0.2	14.9
CopoPP + 10% talc	1440.0 ± 34.5	46.2	31.9 ± 0.4	19.0
CopoPP + 15% talc	1690.0 ± 50.0	71.6	33.2 ± 0.3	23.9
CopoPP + 20% talc	1950.0 ± 67.1	98.0	34.7 ± 0.4	29.5
CopoPP + 15% talc (targeted commercial compound)	1800		28.2	

Table 2. Tensile Modulus and Strength of Talc-Reinforced CopoPP Composites

sample	tensile modulus (MPa)	improvement (%)	tensile strength (MPa)	improvement (%)
neat CopoPP	1140.0 ± 15.7		24.6 ± 0.5	
CopoPP + 5% talc	1318.0 ± 75.4	15.6	24.5 ± 0.3	−0.4
CopoPP + 10% talc	1512.0 ± 55.4	32.6	25.7 ± 0.4	4.2
CopoPP + 15% talc	1882.0 ± 86.4	65.1	23.6 ± 0.4	−4.1
CopoPP + 20% talc	2217.0 ± 27.6	94.5	24.7 ± 0.3	0.4
CopoPP + 15% talc (targeted commercial compound)	2086		22.1	

research, this part was produced from the optimized CopoPP formulation, 49% CopoPP + 45% HomoPP + 4% talc + 1% hybrid + 1% GNP, by using a 700-ton Krauss-Maffei injection machine with the injection parameters (Table S2) without making any modifications in the mold.

2.4. Structural and Thermal FEA Methodology of the B Pillar Interior Part. Structural and thermal modeling of the B pillar interior part was conducted by using FEA methodology with the Simcenter 11.0.0.33 software. Structural and thermal calculations were performed by NX Nastran Solver and NX Thermal Solver, respectively. Figure S5(a) shows the computer-aided model of the B pillar interior part while Figure S5(b) displays its first-boundary conditions. To restrict the movement of the part under the applied mechanical loads, movement in the *X*, *Y*, and *Z* directions was restricted in the holes, shown with orange and purple arrows in Figure S5(b).

The B pillar interior part, the parts that contacted it (reglette, button), and the rigid spheres/objects (RB-rigid bodies) that transmit the loads to the surface were modeled with sticky contact boundary conditions, and the location of the parts and loads are shown in Figure S6. In this configuration, six analyses were conducted for each RB, employing 50 and 100 N loads, as detailed in Table S3, outlining the analysis and corresponding load conditions.

The boundary conditions (restricted freedoms) used in the structural analysis were entirely applied in thermal analysis, as well. The thermal analysis of the B pillar interior part was conducted at 80 °C using tensile test data and defined with an isotropic elastic−plastic material model employing the Paul Dubois cycle. Instantaneous linear thermal expansion coefficients were determined as a function of temperature, averaging the values in the transverse and longitudinal directions within the temperature range of −28 to 120 °C. A linear temperature increase was modeled starting from 23 °C up to an upper-temperature limit of 85 °C. A separable contact definition was established between the relevant components. Heat conduction loss due to contact-related heat transfer between contacting parts was disregarded.

2.5. Part Performance Tests. The B-pillar interior component underwent two performance evaluations: thermal resistance and impact resistance measured using the weight drop method. The part's resistance against temperature was tested at 90 °C for 22 h and the changes in the dimensions of the part before and after the test were noted. On the other hand, the deformation of the part under impact was determined by placing weight on it after conditioning the part in a climatic chamber for 3 h. Moreover, the assembly test involved attaching components slated for assembly with control fixtures (CF) to verify the compatibility of the B pillar interior part with its adjacent components.

2.6. Characterization. The mechanical tests of the prepared CopoPP composites were performed via a 5982 Static universal test machine (UTM, Instron, Norwood, MA, USA) with a 5 kN load cell for ISO 527-2 tensile, ISO 178 three-point bending, and ISO 179 charpy-impact tests. Dynamic mechanical analysis (DMA) of the samples was conducted by using the Mettler Toledo DMA1 dynamic mechanical analyzer (Columbus, OH, USA) at 1 Hz and between −60 and 160 °C at a heating rate of 3 °C/min. In addition, storage modulus (E'), loss modulus (E''), and tan δ values from DMA analysis were calculated by using STARe software (Mettler Toledo, Columbus, OH, USA). Thermal features of the samples were determined under an inert atmosphere by differential scanning calorimetry (DSC) analysis by heating from 20 to 200 °C at a heating rate of 10 °C/min and holding at 200 °C for 5 min by using a Mettler Toledo DSC 3 + 700. The rheological characteristics of the samples were examined by using an MCR 702 TwinDrive Rheometer (Anton Paar, Graz, Austria) at 210 °C under a nitrogen atmosphere (N_2). The surface features of the cross-section of the samples were determined by a field emission scanning electron microscope (FESEM, Leo Supra 35VP, Carl Zeiss AG, Jena, Germany). Finally, the life cycle assessment (LCA) study was carried out by using Simapro software (9.3.0.2 release) with its Ecoinvent 3-allocation cut off by classification, and system library.

3. RESULTS AND DISCUSSION

3.1. Effect of Talc and Waste-Driven GNP in the Developed CopoPP-Based Compound Formulation. It is known that reinforcing PP with talc and further increasing its content enhance the mechanical characteristics of the final PP composites due to the enhanced level of crystallinity within the composite.[32−34] In this research, CopoPP composite was also reinforced with talc by increasing its ratio from 5 to 20 wt % and the resultant flexural and tensile features are summarized

https://doi.org/10.1021/acsomega.4c02596
ACS Omega 2024, 9, 34530−34543

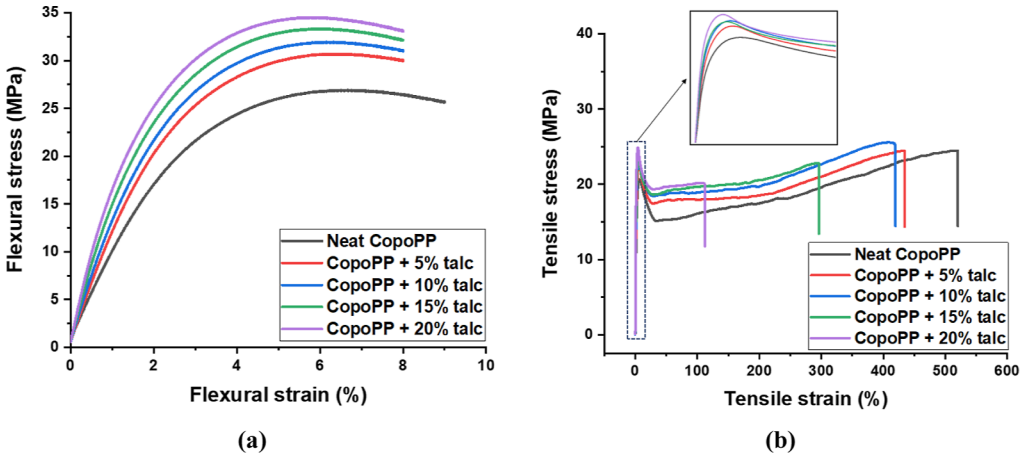

Figure 1. (a) Flexural and (b) tensile stress−strain curves of CopoPP composites loaded with talc between the amounts of 5−20 wt %.

Table 3. Flexural Modulus and Strength of CopoPP Composites Reinforced with Different Combinations of HomoPP, Talc, Hybrid Additive, and GNP

sample	flexural modulus (MPa)	improvement (%)	flexural strength (MPa)	improvement (%)
neat CopoPP	985.0 ± 25.1		26.8 ± 0.1	
CopoPP + 1% GNP	1080.0 ± 15.0	9.6	29.5 ± 0.1	10.1
CopoPP + 5% talc	1260.0 ± 20.4	27.9	30.8 ± 0.2	14.9
CopoPP + 1% hybrid	1037.0 ± 39.7	5.3	28.2 ± 0.7	5.2
80% CopoPP + 20% HomoPP	1190.0 ± 48.4	20.8	33.2 ± 0.5	23.9
50% CopoPP + 50% HomoPP	1400.0 ± 51.5	42.1	38.8 ± 0.4	44.8
49% CopoPP + 45% HomoPP + 4% talc + 1% hybrid + 1% GNP	1700.0 ± 50.1	72.6	42.8 ± 0.5	59.7

Table 4. Tensile Modulus and Strength of CopoPP Composites Reinforced with Different Combinations of HomoPP, Talc, Hybrid Additive, and GNP

sample	tensile modulus (MPa)	improvement (%)	tensile strength (MPa)	improvement (%)
neat CopoPP	1140.0 ± 15.7		24.6 ± 0.5	
CopoPP + 1% GNP	1274.0 ± 44.4	11.8	25.4 ± 1.3	3.3
CopoPP + 5% talc	1318.0 ± 75.4	15.6	24.5 ± 0.3	−0.4
CopoPP + 1% hybrid	1051.8 ± 87.8	−7.8	24.5 ± 0.1	−0.4
80% CopoPP + 20% HomoPP	1356.0 ± 90.0	18.9	29.6 ± 0.2	20.3
50% CopoPP + 50% HomoPP	1578.0 ± 22.9	38.4	35.5 ± 0.3	44.3
49% CopoPP + 45% HomoPP + 4% talc + 1% hybrid + 1% GNP	1731.3 ± 158.3	51.9	30.6 ± 0.7	24.4

in Tables 1 and 2, respectively, along with those of the commercial CopoPP composite containing 15 wt % of talc. As consistent with the literature,[35] the inclusion of talc in CopoPP resulted in an enhancement of both the flexural modulus and strength of the composite, showing a directly proportional increase with the loading ratio. The incorporation of 5 wt % talc resulted in an approximate improvement of 27.9% in flexural modulus and boosted up to 98.0% by increasing the talc content to 20 wt %. The same trend was also observed in the flexural strength of the CopoPP composites. The advancement of the flexural strength of CopoPP was 14.9% for 5 wt % talc presence and it reached 29.5% for 20 wt % talc inclusion. Talc's platy structure acts as a strong internal reinforcement within the PP matrix. During processing, these platelets align with the flow direction, potentially causing a similar alignment of PP polymer chains, improving the flexural properties. On the other hand, the tensile modulus of CopoPP steadily increased, ranging from 15.6 to 94.5% with the talc content ratio, changing from 5 to 20 wt %. The higher modulus values are due to the restricted mobility of polymeric chains resulting from the talc existence.[36] However, the tensile strength of the CopoPP decreased by 0.4 and 4.1% in the presence of 5 and 15 wt % talc, respectively, which might stem from the increased material stiffness resulting from the talc inclusion.[36] The highest tensile strength was achieved by the incorporation of 10 wt % talc with an enhancement of 4.2%. This can be ascribed to the formation of stress concentration zones surrounding the talc particles, thereby lessening the stress transfer between the matrix and the filler.[37−39]

Furthermore, Figure 1 displays the flexural and tensile stress−strain curves of CopoPP composites loaded with 5−20 wt % talc. The talc-reinforced composites exhibited a higher Young's modulus compared to the neat CopoPP, represented by the initial slope in the elastic region of the graph, increasing with the increased talc concentration due to the stiffness of talc.[40] However, as a result of the increased stiffness (elastic modulus), a noteworthy reduction occurred in the elongation at the break of the CopoPP composites. This phenomenon can be attributed to the role of talc acting as a stress concentrator related to its particle size and distribution, thereby accelerating quicker failure during the tensile test.[41]

https://doi.org/10.1021/acsomega.4c02596
ACS Omega 2024, 9, 34530−34543

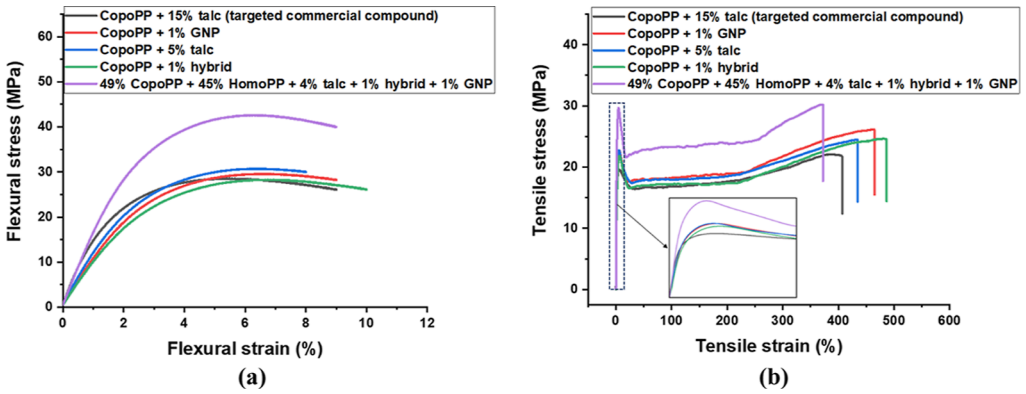

Figure 2. (a) Flexural and (b) tensile stress−strain curves of the CopoPP composites reinforced with different additives and the developed CopoPP formulation along with the commercial targeted compound.

Table 5. Comparison of the Flexural and Tensile Properties, Density, and Impact Energy of the Commercial, Newly Developed, and Recycled CopoPP Formulations

	flexural modulus (MPa)	flexural strength (MPa)	tensile modulus (MPa)	tensile strength (MPa)	density (g/cm^3)	impact Energy (charpy-notched) (kJ/m^2)
CopoPP + 15% talc (commercial one)	1800.0	28.2	2086.0	22.1	1.02	30.00
49% CopoPP + 45% HomoPP + 4% talc + 1% hybrid + 1% GNP (the newly developed one)	1700.0	42.8	1731.3	30.6	0.92	5.84
recycled PP + 4% talc + 1% hybrid + 1% GNP	1425.0	35.1	1385.7	25.1	0.93	6.38

Since it was aimed to achieve a 10 wt % reduction in weight and enhanced mechanical characteristics in the final CopoPP-based composite within this research, talc content was decreased, and graphene/talc hybrid and GNP were included in the CopoPP structure. Furthermore, the influence of interaction between HomoPP and CopoPP on the ultimate flexural and tensile properties of the resulting composites was investigated. Tables 3 and 4 present the summary of the flexural and tensile test results obtained for different additive loadings in CopoPP composites. Initially, the effect of incorporating GNP at a low concentration into the CopoPP matrix was investigated. Even a minor addition of 1 wt % GNP led to approximately 9.6 and 10.1% enhancements in the flexural modulus and strength of the CopoPP composite. Due to the large surface area of GNP, increased contact area with the matrix is provided. This maximized interface facilitates efficient stress transfer between the matrix and the GNP, ultimately leading to improved flexural performance of the composites. Furthermore, using 1 wt % hybrid additive in the CopoPP composite rather than 1 wt % GNP increased the flexural modulus and strength of the composite by nearly 5%. Therefore, in order to improve the flexural characteristics of the final CopoPP composite, talc, hybrid additive and GNP were used together to create a synergistic effect between the additives.

Moreover, to further enhance the interaction between the polymer matrix and additives, and leverage the superior mechanical properties and crystallinity of HomoPP, the formulation was modified by blending HomoPP with CopoPP. An initial exploration identified a 20 wt % HomoPP addition to the CopoPP matrix as optimal, which resulted in 20.8 and 23.9% in flexural modulus and strength, respectively. By increasing the HomoPP ratio to 50 wt % in the HomoPP/CopoPP blend, 42.1 and 44.8% advancements were observed in the flexural modulus and strength, respectively. However, since CopoPP must be the dominant polymer matrix in the ultimate composite, 49% CopoPP + 45% HomoPP + 4% talc + 1% hybrid + 1% GNP composite formulation was specified, which resulted in 72.6 and 59.7% enhancements in flexural modulus and strength, respectively.

Regarding the tensile characteristics of the CopoPP composites (Table 3), the existence of GNP made 11.8 and 3.3% enhancements in tensile modulus and strength, respectively, lower than the values obtained by 5 wt % talc inclusion. On the other hand, the addition of 1 wt % hybrid additive in CopoPP composite caused a reduction in both tensile modulus and strength of the composite. However, the tensile modulus and strength were enhanced by 51.9 and 24.4%, respectively, using the developed CopoPP formulation. These improvements were attributed to the effective stress transfer between the polymer matrix and the additives supplied from the inherent stiffness of the PP homopolymer, and the substantial surface area provided by GNP.[42−44] Furthermore, the natural platelet-like shape of GNP allows them to make closer contact with the neighboring platelets when evenly distributed. This, in turn, promotes more effective stress transfer between the matrix and fillers, leading to improved mechanical properties.[44] Consequently, it became evident that incorporating both talc, hybrid additive, and GNP into the CopoPP composite structure yielded more favorable results compared to adding them separately.

Figure 2 shows the stress−strain curves of the CopoPP composites reinforced with GNP, talc, and hybrid additive, separately, and the developed CopoPP formulation along with the commercial targeted compound. The incorporation of additives to CopoPP generally led to a reduction in the elongation at break. The decrease in elongation at break also observed in the optimized CopoPP formulation can be attributed to the presence of rigid fillers that created significant discontinuities in the matrix. Consequently, the actual elongation experienced by the polymer matrix was considerably greater than the measured elongation of the specimen,

https://doi.org/10.1021/acsomega.4c02596
ACS Omega 2024, 9, 34530−34543

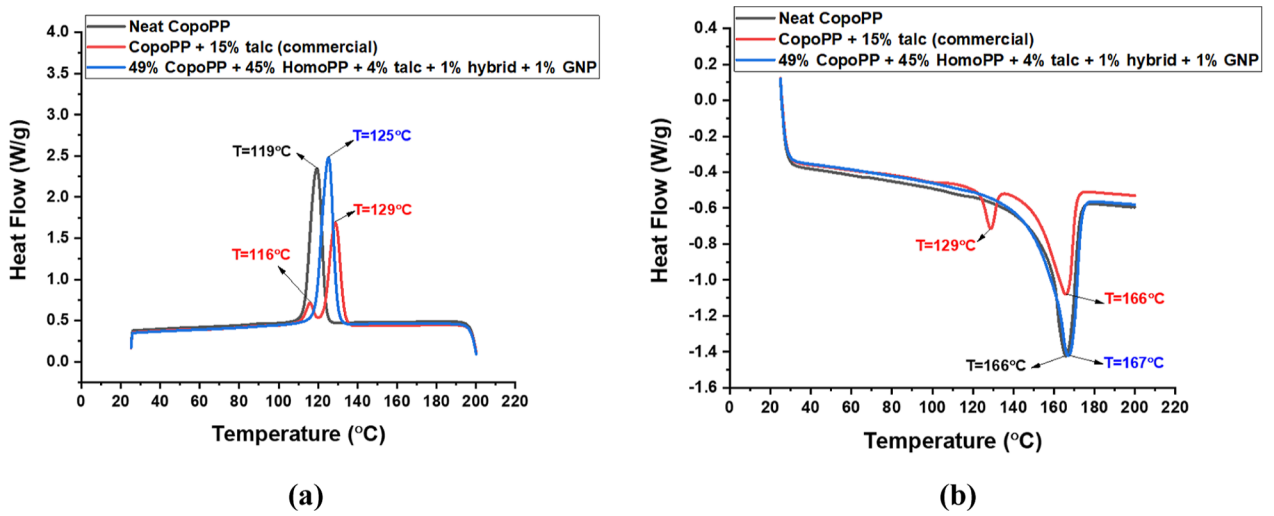

Figure 3. (a) Crystallization curves in the first cooling cycle and (b) melting curves in the second heating cycle of neat, commercially available, and newly developed CopoPP composites.

indicating that all elongation originated from the matrix.[45] Notably, the optimized CopoPP formulation yielded significantly higher improvements in both flexural and tensile stress−strain curves. The synergistic combination of talc, hybrid additive, and GNPs in the CopoPP composite led to enhanced stiffness and ultimately the highest mechanical strength among composites containing only one of these additives.

3.2. Benchmarking Study of the Developed CopoPP-Based Compound with the Commercially Available CopoPP Compound. In order to assess the potential of the newly developed CopoPP-based compound formulation as an alternative to the commercially available counterpart, a comparison of their tensile, flexural, impact characteristics, and density values was conducted and is presented in Table 5. Moreover, the substitution of virgin PP with recycled PP was considered and a comparative display of their mechanical characteristics and density is presented in Table 5. The higher flexural and tensile strength values in the newly developed CopoPP revealed the enhanced capacity to resist deformation under compression and tension load.[46] The flexural and tensile modulus of the commercially available CopoPP and the newly developed CopoPP were more or less the same although there was a huge difference in their impact energies due to introducing HomoPP to the newly developed CopoPP formulation. On the other hand, the flexural and tensile modulus of the recycled CopoPP-based composite was lower than that of the other two composites, signaling reduced stiffness under tensile stresses. However, the flexural and tensile strength of recycled PP-based composite outperformed the commercial counterpart, yet the newly developed CopoPP-based one emerged as the most robust choice, exhibiting exceptional resistance to bending and load-induced failure. Moreover, the impact energy of the recycled PP-based composite closely resembled that of the newly developed CopoPP-based composite, but it was nearly five times lower than that of the commercially available CopoPP composite. On the other hand, as desired, nearly 10% weight reduction was supplied both with the newly designed CopoPP-based and recycled PP-based formulations compared to the commercially available one. In summary, the recycled PP composite offered a well-balanced combination of strength and impact resistance. In contrast, the newly developed composite delivered high strength while maintaining stiffness levels similar to the commercial CopoPP composite. Thus, it can be concluded that the "49% CopoPP + 45% HomoPP + 4% talc + 1% hybrid + 1% GNP" formulation can be the most comparable candidate to the commercially available CopoPP composite.

Furthermore, the crystallinity of polymers can have a profound impact on properties such as mechanical strength and stiffness of the final composite.[47] Therefore, it is crucial to investigate the effect of the addition of different additives on the polymer's crystallization behavior. The thermal behavior of the neat CopoPP and the reinforced CopoPP composites was evaluated using DSC analysis. Figure 3 shows the melting and the crystallization peaks of the DSC curves of neat CopoPP, CopoPP + 15% talc (commercial), and the "49% CopoPP + 45% HomoPP + 4% talc + 1% hybrid + 1% GNP" composites obtained from first cooling and second heating cycles while Table 6 provides the DSC results of the melting peak temperature (T_m), melting enthalpy (ΔH_m), crystallization peak temperature (T_c), crystallization enthalpy (ΔH_c), and crystallinity percentage (X_c) of the neat and reinforced CopoPP composites. X_c was calculated based on eq 1, where ΔH_m is the melting enthalpy of the samples, w represents the weight fraction of the PP phase and ΔH_m° is the theoretical melting enthalpy of 100% crystalline PP taken as 207 J/g for HomoPP and 190 J/g for CopoPP.[48,49]

Table 6. Summary of the Thermal Parameters of Neat, Commercially Available and the Newly Developed CopoPP Composites Obtained from DSC Characterization

sample	T_m (°C)	ΔH_m (J/g)	T_c (°C)	ΔH_c (J/g)	X_c (%)
neat CopoPP	166	77.0	119	79.6	40.5
CopoPP + 15% talc (commercial)	166	54.6	129	51.4	33.8
49% CopoPP + 45% HomoPP + 4% talc + 1% hybrid + 1% GNP	167	88.8	125	88.1	47.44

$$X_c = \frac{\Delta H_m}{\Delta H_m^\circ \times w} \times 100 \quad (1)$$

No noticeable difference was observed in the T_m of the CopoPP composites when various additives were incorporated,

https://doi.org/10.1021/acsomega.4c02596
ACS Omega 2024, 9, 34530−34543

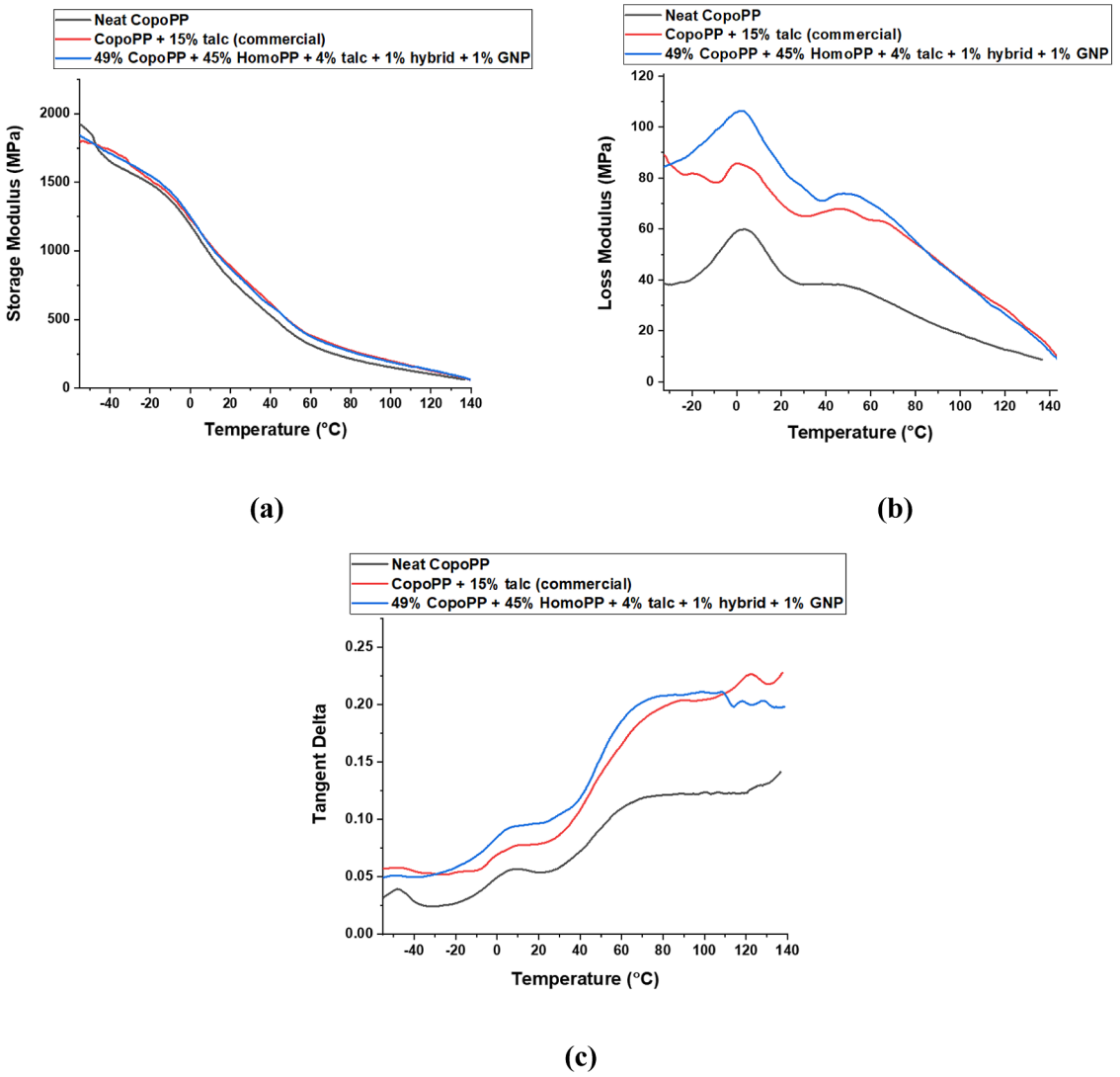

Figure 4. (a) Storage modulus, (b) loss modulus, and (c) tangent delta of neat CopoPP, commercially available CopoPP, and the optimized CopoPP composite as a function of temperature.

indicating that the crystal structure of PP remained constant despite the addition of talc, hybrid additive, and GNP.[41,50] Similar results were reported by Sarturato et al.[49] However, it is worth noting that the commercially available CopoPP sample exhibited a double melting peak, underscoring the significant influence of crystal forms on T_m. In miscible polymer blends, the uniform mixing of polymer components at a molecular level creates a single-phase system, and the properties of miscible blends are a combination of the properties of their pure components. The crystallization and melting behavior of such blends can be complex, influenced by several factors such as component structure, molecular weight, concentration, and intermolecular interactions.[51] In the developed compound, when CopoPP and HomoPP were blended, their crystallization and melting behavior mimicked that of a single, homogeneous polymer resulting in a single crystallization and melting peak in DSC thermographs due to their similar chemical structure. On the other hand, as the difference between the T_m of two components was small, they could be crystallized simultaneously.[52] In addition, the cooling rate could also have a significant impact on the DSC thermographs of the blends.[53] The alteration in the melting enthalpy measurements of both the commercial and newly developed samples highlighted the impact of additive integration on the polymer matrix's crystalline structure. The heightened enthalpy values observed in the optimized CopoPP sample suggested that GNP restricted the mobility of polymer chains, thereby increasing the energy needed to induce phase transitions within the composite.[54] Conversely, the reduction in ΔH_m of the commercially available CopoPP composite in comparison to the neat CopoPP indicated that the inclusion of substantial talc content in the PP matrix introduced defects into the polymer's crystal lattice.[55] Comparing the neat CopoPP composite with the commercial and the newly developed CopoPP-based composites, there was an increase of 10 and 6 °C in the crystallization temperature, respectively. This increase in the T_c indicated faster crystallization of polymer chains after cooling and the nucleating effect of the fillers.[36] The commercially available CopoPP composite had a 16.5% lower crystallinity degree than that of neat CopoPP while the newly developed CopoPP-based composite exhibited a 17.1% increase, which was attributed to the small size and low concentration of the employed GNP serving a seed for heterogeneous nucleation, thus favoring the crystallinity degree

https://doi.org/10.1021/acsomega.4c02596
ACS Omega 2024, 9, 34530−34543

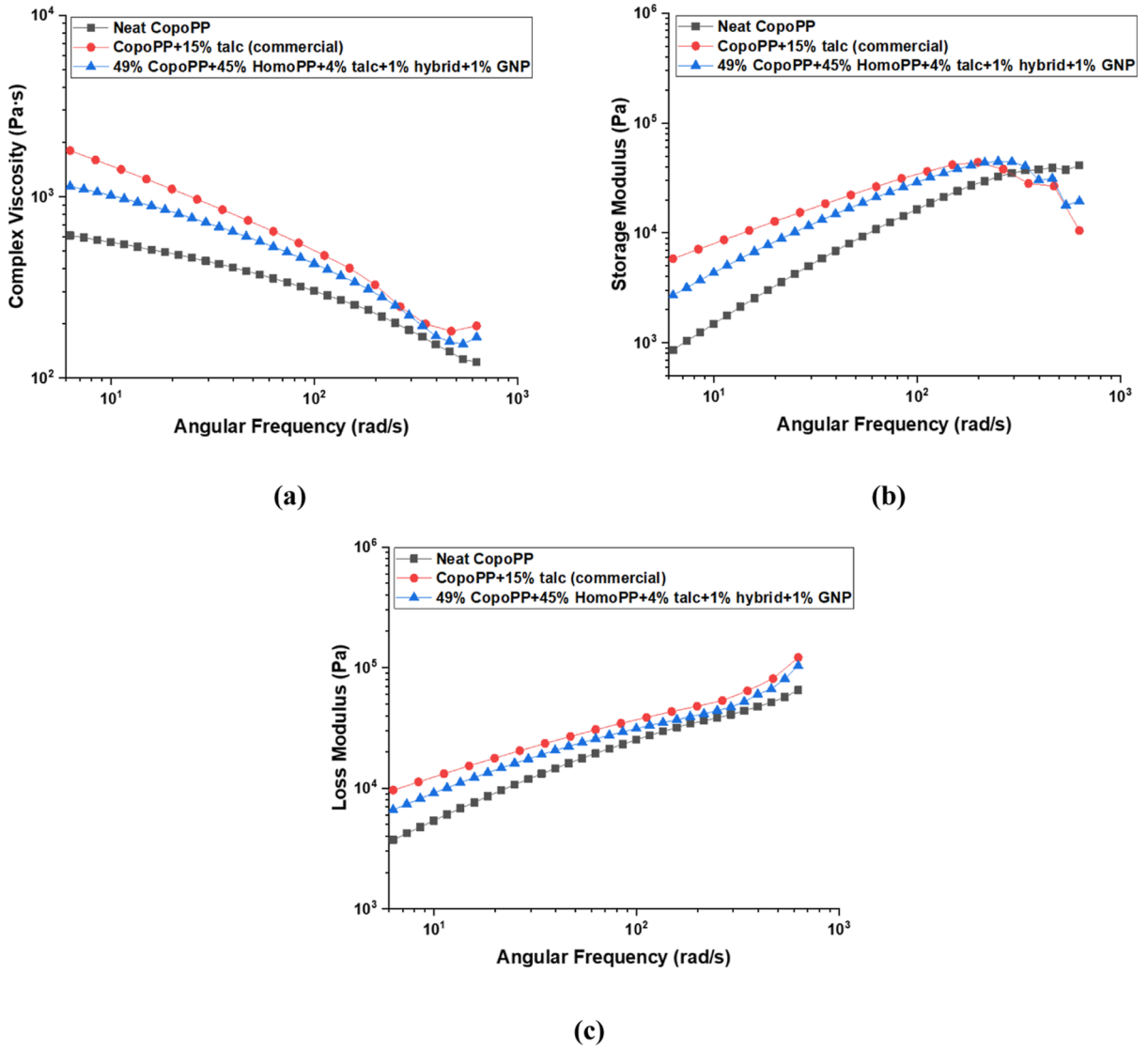

Figure 5. Rheological behavior of neat CopoPP, CopoPP + 15% talc (commercially available), and the "49% CopoPP + 45% HomoPP + 4% talc + 1% hybrid + 1% GNP" (a) complex viscosity (η^*), (b) shear storage modulus (G'), (c) shear loss modulus (G'') curves.

of the final composite.[56] Therefore, the nucleating ability of the additives incorporated into the newly developed CopoPP-based was confirmed by the higher T_c, followed by a higher crystallinity degree, which contributed to the increase in the modulus and the retention of the strength of the resultant composite.

3.3. Interface Relations of the Reinforcements with the CopoPP Matrix. The interface relations of the reinforcements with the polymer matrix were examined by DMA and the storage modulus (E'), loss modulus (E'') and tangent delta value curves of neat CopoPP, CopoPP + 15% talc (commercial) composite, and the optimized "49% CopoPP + 45% HomoPP + 4% talc + 1% hybrid + 1% GNP" composites as a function of temperature are presented in Figure 4. The storage modulus of CopoPP as well as its reinforced composites decreased with an increase in temperature, which was mainly attributed to the effect of temperature on the mobility and arrangement of polymer chains within the material.[57] The E' curves of both the commercial and optimized CopoPP composites exhibited a slightly higher storage modulus, indicating that the addition of talc, hybrid additive, and GNP contributed to a reinforcing effect. This enhancement primarily depended on two factors which were the aspect ratio of the dispersed nanoparticles and the effectiveness of polymer chain integration with the additives.[58] When the CopoPP matrix was strengthened with talc, hybrid additive and GNP, the polymer interface near these particles was subjected to increased mechanical restraint. In addition, platelet edges of the talc and hybrid additive particle acted as weak points accumulating high stress concentrations within the polymer matrix.[50] However, by the incorporation of GNP, these weak points were diminished, facilitating a more extensive and uniform transfer of stress between the polymer matrix and the filler particles due to its high aspect ratio.[59]

On the other hand, the loss modulus curves in Figure 4b showed two significant transitions. The first transition occurred at around 10 °C in all composites corresponding to the glass transition temperature (T_g) of the CopoPP-based composites. Notably, there was no noteworthy change in the T_g peak positions of the composites. The second transition, observed in the 40−60 °C range, was the α transition, associated with the relaxation of restricted amorphous chains in the crystalline

https://doi.org/10.1021/acsomega.4c02596
ACS Omega 2024, 9, 34530−34543

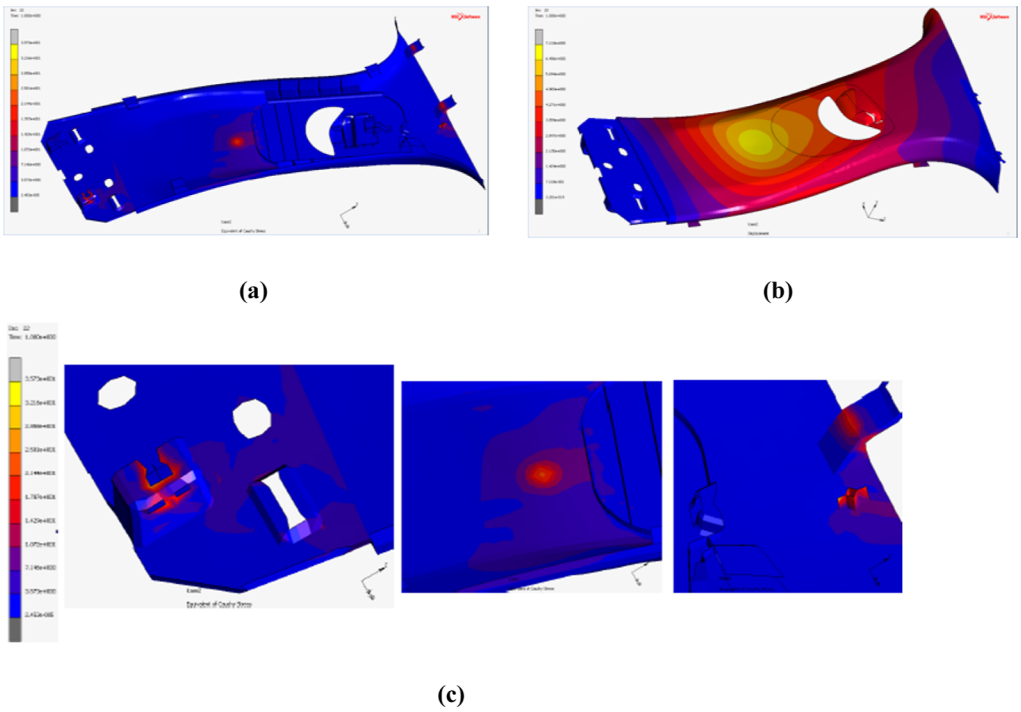

Figure 6. (a) Cauchy stress and (b) displacement maps formed on the part in the run "4" condition, and (c) closer images of the maximum displacements that occurred in the nail areas.

phase, known as rigid amorphous molecules. It was more pronounced in the optimized CopoPP composite and the increased intensity of this transition in the reinforced CopoPP composites suggested a higher presence of amorphous phase.[60] Overall, the loss modulus of both the commercial and optimized CopoPP composites was higher than that of the neat CopoPP because of the increased internal friction facilitating the dissipation of energy.[61]

Based on the tan δ spectra of the composites, shown in Figure 4c, the reinforced CopoPP composites showed higher damping than neat CopoPP, indicating increased energy dissipation in the presence of additives. Importantly, this parameter was a valuable tool for distinguishing differences in the viscoelasticity of materials, regardless of materials' stiffness.[60] The highest tan δ peak height in the optimized CopoPP composite suggested greater energy dissipation and a higher level of stress transfer between the fillers and the polymer matrix.[62] This typically indicated strong filler−matrix interactions and successful reinforcement impact in the optimized "49% CopoPP + 45% HomoPP + 4% talc + 1% hybrid + 1% GNP" CopoPP composite.[58]

Furthermore, the dispersion of the reinforcements in the CopoPP matrix and their interaction with the CopoPP were examined from the cross-sectional fracture surfaces by using SEM analysis. Cross-sectional fracture surfaces of neat CopoPP, CopoPP with 15% talc (commercially available), and the optimized CopoPP composite containing 49% CopoPP, 45% HomoPP, 4% talc, 1% hybrid, and 1% GNP are presented in Figure S7. As seen in Figure S7(a), neat CopoPP displayed a smoother fracture surface but exhibited some voids within its structure due to the presence of ethylene groups. These voids could contribute to lower the mechanical properties of the composite.[28] Conversely, the addition of additives can result in a more brittle structure, as the talc particles act as stress concentrators.[63] Additionally, the strong interaction between the lamellar structure of talc and the polymer matrix along with the uniform surface roughness in the fracture surface of commercial CopoPP and the optimized CopoPP composites indicated homogeneous and proper dispersion of additives within the CopoPP matrix. The development of robust interphase and enhanced adhesion between the matrix and the reinforcements were also supported by the significant improvement in tensile strength observed in the developed formulation compound.

3.4. Rheological Characterization of the CopoPP Composites Regarding the Reinforcement Type. The rheological behavior of polymers or polymer-based nanocomposites plays a vital role in their microstructure and processability.[64] The viscoelastic characteristics of neat CopoPP, CopoPP + 15% talc (commercially available), and the optimized composite consisting of 49% CopoPP, 45% HomoPP, 4% talc, 1% hybrid, and 1% GNP are illustrated in Figure 5. These properties are presented in terms of complex viscosity (η^*), storage modulus (G'), and loss modulus (G'') as functions of angular frequency at a melt temperature of 210 °C. Neat CopoPP exhibited typical thermoplastic behavior, followed by shear-thinning behavior as the frequency increased, as shown in Figure 5a. This indicated that the viscosity of the composite decreased with rising frequency, signifying restricted mobility of CopoPP chains when reinforced with talc, hybrid, and GNP at low frequencies. Conversely, higher shear forces at elevated frequencies enabled the polymer chains to flow more freely. At lower frequencies, the introduction of rigid reinforcements led to an increase in the G' due to the presence of well-dispersed and properly bonded reinforcements, resulting in enhanced stiffness and strength of the polymer matrix. This rise in the G' reflected the improved elastic behavior and increased resistance to deformation at low strain rates. Figure 5b demonstrated the higher G' values of the reinforced composites in comparison to

https://doi.org/10.1021/acsomega.4c02596
ACS Omega 2024, 9, 34530−34543

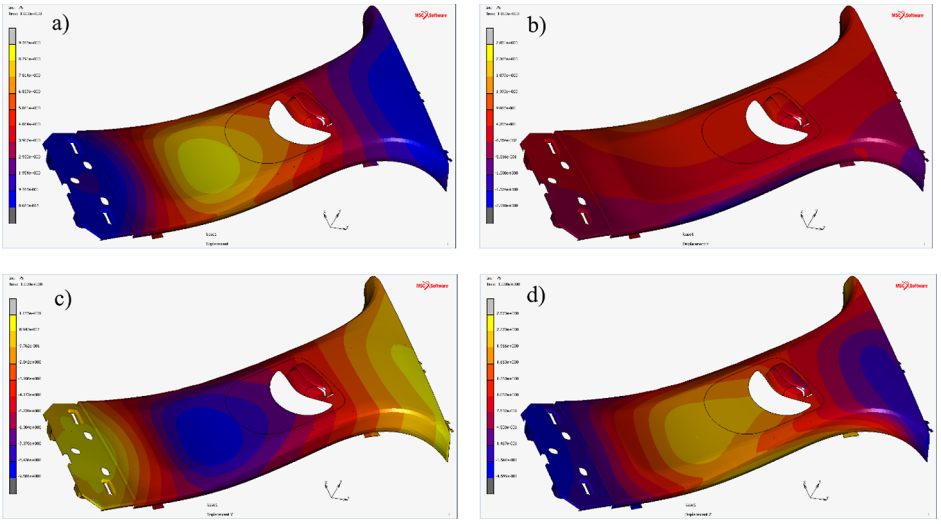

Figure 7. Displacement distribution of the automotive part under thermal load: (a) total displacement, (b) displacement in *X* direction, (c) displacement in *Y* direction, and (d) displacement in *Z* direction.

the neat CopoPP attributed to the presence of rigid fillers. The increased rigidity could also be explained by the formation of an interphase between the polymer matrix and the rigid fillers, resulting in intermediate rigidity between that of talc and CopoPP.[65] According to Figure 5c, the loss modulus of all materials increased up to a certain frequency. However, at high frequencies, approximately around 100 rad/s, the storage modulus decreased in CopoPP-based composites containing talc, talc/GNP, and hybrid additives, while the *G″* continued to rise. This phenomenon may be induced by the high shear rate, which disrupted the interface interaction between the fillers and polymer matrices. The results underscored that the newly developed composite "49% CopoPP + 45% HomoPP + 4% talc + 1% hybrid + 1% GNP" exhibited melt processability similar to that of commercially available CopoPP composite, as well as neat CopoPP. This similarity highlighted its potential to be an alternative material to the commercial composite.

3.5. B-Pillar Interior Prototype Part Development. The B pillar interior part was manufactured using the optimized CopoPP compound formulation, 49% CopoPP + 45% HomoPP + 4% talc + 1% graphene/talc + 1% GNP, through injection molding without making any change in the mold design. In serial production, the B pillar interior is typically fabricated from the commercial compound that is 15% talc-reinforced CopoPP. While the weight of the part produced using the commercial compound was 320 g, it was reduced to 290 g with the newly manufactured B pillar interior part, representing a 9.4% reduction in part weight. Table S4 provides a summary of the weight differences between the B pillar interior parts produced from the commercial compound and the newly developed compound formula.

3.6. Thermal and Structural FEA Findings of the B-Pillar Interior Part. Based on the structural FEA of the B pillar interior part, the maximum displacement and Cauchy stress values obtained with the SEA program for each load case are presented in Table S5. During the simulation tests, the maximum Cauchy stress was 35.7 MPa and the maximum displacement was 7.1 mm in the load-condition "4" in realistic loading, and the stress and displacement maps formed on the part are given in Figure 6. In Figure 6a, the maximum displacement in the concentrated load region on the lower surface of the part could be seen. In addition, maximum displacements occurred in the nail areas where the part held onto other parts. These parts can be seen closely in Figure 6c.

According to the thermal analysis results, the total displacement on the part and the displacements in the *X*, *Y*, and Z directions are shown in Figure 7. In Figure 7a the examination of the displacement distribution of the part can be seen. Figure 7b shows the displacement distribution occurred only in the *X* direction. In this direction, the displacement distribution was obtained close to homogeneous. The distribution in the *Y* direction Figure 7c was at higher values in areas where the part was fixed. Lastly, Figure 7d shows the displacement in the *Z* direction. The highest displacement occurred in the curved middle region. Accordingly, the largest displacement was 9.77 mm observed under 85 °C.

3.7. Part Performance Analysis. Based on the temperature resistance test, since the part showed less than 0.4% deformation before and after the test, the part passed the test successfully. On the other hand, the B pillar interior part successfully passed the impact test with the weight drop method since there were no broken pieces on the part at the end of the test. In Table S6, the test results of temperature resistance and impact test with weight drop method are summarized. Furthermore, to check the compatibility of the B pillar interior part with the neighboring parts, the assembly process (CF) test was carried out with the parts to be assembled. The newly developed CopoPP-based B pillar interior part has not passed this test yet, however, it is expected that after optimization studies regarding the injection process parameters specific to this test are conducted, the part will pass the test.

3.8. Comparative LCA Study of the Developed Compound and B-Pillar Interior Part. LCA was conducted to assess and compare the environmental impacts of the CopoPP composites. For the life cycle inventory, Ecoinvent 3 was employed, utilizing allocation cutoff by classification and Swiss input and output databases. To compute the environmental impacts, SimaPro software version 9.3.0.2 was utilized. This assessment incorporated inputs measured in mass units when assessing waste disposal scenarios, disregarding volume units. The scenario followed a cradle-to-grave approach, assuming landfilling in a municipal solid waste facility as the final disposal method that was taken from the software (Figure

https://doi.org/10.1021/acsomega.4c02596
ACS Omega 2024, 9, 34530−34543

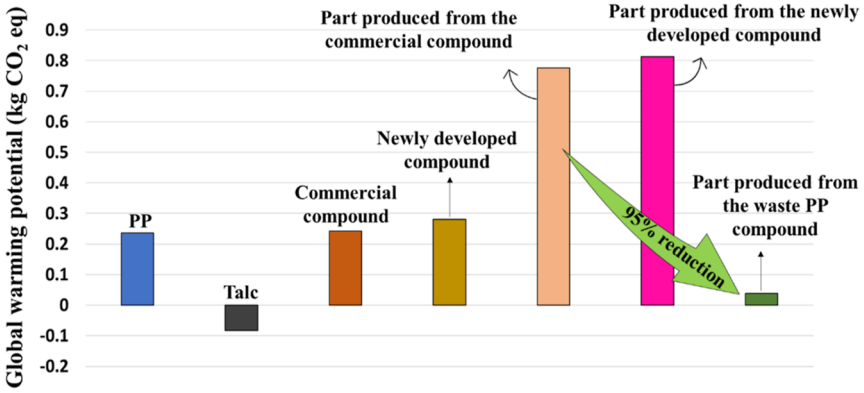

Figure 8. Global warming potentials of PP, talc, commercially available compound, the newly developed compound, B pillar interior part obtained from these compounds, and the global warming potential in case of waste PP utilization.

S8). The cradle stage starts with the raw materials being prepared in the lab, specifically for compound preparation. Given that the production of hybrids involved using waste PP as an input, only the transportation of waste PP was taken into consideration. Various environmental impact categories such as ozone depletion, global warming, smog, acidification, eutrophication, carcinogenicity, noncarcinogenicity, respiratory effects, ecotoxicity, and fossil fuel depletion were evaluated within this study. In addition, the comparison of impact assessments for the inputs was determined using a method that incorporates equivalence factors from the Intergovernmental Panel on Climate Change.

LCA of neat CopoPP, talc, CopoPP + 15% talc, and the newly developed "49% CopoPP + 45% HomoPP + 4% talc + 1% hybrid + 1% GNP" compounds were conducted, and various environmental impacts such as global warming potential, acidification, eutrophication, ozone depletion, human toxicity, ecotoxicity, human health, and agricultural land use were evaluated and presented in Table S7. Among these impacts, global warming potential was given particular importance within the scope of this work. According to Table S7, the commercially available CopoPP compound filled with 15 wt % talc had a 2.61% higher CO_2 footprint compared to the neat CopoPP. In addition, the optimized "49% CopoPP + 45% HomoPP + 4% talc + 1% hybrid + 1% GNP" compound formulation, despite its 10% weight reduction, showed a 15.71% higher global warming potential than the commercially available "PP + 15% talc" compound. This increase was due to the higher PP content and lower talc content in the optimized compound formulation. Since talc had a negative global warming potential, reducing its amount resulted in an increased global warming potential. Furthermore, the environmental impacts of the B pillar interior part produced from the commercially available PP-based compound and the newly developed PP-based compound were also evaluated and compared in Table S8. Since CO_2 emissions of the newly developed PP-based compound were higher than those of the commercially available compound used in serial production, higher CO_2 emission was observed for the newly developed B pillar interior part compared to the one from in serial production. However, the innovative formulation of the PP-based part compound allowed for a 10% reduction in weight without requiring any modifications to the injection mold. This weight reduction will correspond to a 10% decrease in the vehicle's final CO_2 emissions released into the atmosphere. It is important to note that the higher CO_2 emission values in the LCA studies for the newly developed CopoPP-based compound and B pillar interior part produced from the developed compound should not be misinterpreted as a failure of the newly developed components to offer environmental benefits. Moreover, utilizing waste PP instead of first-grade PP during the part production phase will further reduce CO_2 emissions of the B pillar interior part produced from the newly developed CopoPP-based compound formulation. This was also reported by Melo de Lima et al. that the weight reduction achieved in their PP-based GNP nanocomposite resulted in energy and emissions savings, especially during the automotive part use stage, which is the stage with the most significant contribution in most environmental impact categories.[66] In addition, the global warming potential of graphene/talc hybrid (3.29 kg CO_2 equiv) and upcycled GNP (45.30 kg CO_2 equiv) used in this study is much less than the Commercial GNP which is 101 kg CO_2 equiv[29] Figure 8 presents comparative graphs of the global warming potentials of the commercially available PP-based compound, the newly developed PP-based compound, the automotive part obtained from both compounds and the global warming potential when waste PP is utilized. As shown in Figure 8, the CO_2 emissions of the part produced using waste PP decreased by 95% compared to the part produced using commercial PP + 15% talc compound. Building on these results, future studies are planned to explore the use of waste PP instead of virgin PP.

4. CONCLUSIONS

In the present study, a sustainable approach was pursued for the production of lightweight automotive parts using PP compound by synergistic incorporation of talc, waste tire-driven graphene, and waste plastics-driven graphene/talc hybrid additives. The reinforced CopoPP composite was manufactured by employing a high-shear mixing technique at 180 °C and 4000 rpm with varying loadings of additives. The new compound formulation containing 49% CopoPP, 45% HomoPP, 4% talc, 1% hybrid additive, and 1% GNP was developed to reduce density while preserving the desired mechanical properties, aiming to serve as viable alternatives to the commercial 15% talc-filled CopoPP composite. The developed formulation for the CopoPP compound resulted in a 52 and 38% increase in flexural and tensile strength, respectively, compared to the conventional compound used in automotive part production. These remarkable enhancements can be attributed to the synergistic effects of the incorporated additives. Furthermore, the enhanced degree of crystallinity in

https://doi.org/10.1021/acsomega.4c02596
ACS Omega 2024, 9, 34530−34543

the developed CopoPP compound is attributed to the nucleating effect of GNPs. The crystallinity of PP composites significantly influences their mechanical and thermal properties. Additionally, interface analysis demonstrated enhanced interfacial adhesion and robust interactions between the additives and PP matrices in the developed compounds compared to the commercial ones. This enhanced interaction facilitated efficient stress transfer between the fillers and the polymer matrix, leading to effective reinforcement. The developed compound formulation was successfully utilized to produce the B pillar interior automotive part via injection molding. Subsequently, the thermal and structural characteristics of the produced automotive part were analyzed using finite element methods, and its performance was evaluated through several tests, demonstrating its suitability for mass production. The desired 10% weight reduction was successfully achieved leading to consequently 10 wt % weight reduction in the B pillar interior parts produced from this developed compound which is expected to contribute to the development of lightweight vehicles and result in reduced fuel consumption and overall CO_2 footprint over the vehicle's lifetime. Furthermore, the incorporation of waste PP into the newly developed compound formulation demonstrated significant CO_2 emission reductions of 95% during part production. Overall, this research has enabled the development of compounds that strike a balance between lightweight design, robust mechanical attributes, and thermal stability, providing viable alternatives to commercial compounds for serial part production.

Future research directions could include a comprehensive cost analysis to assess the economic viability of this composite compared to traditional materials. Additionally, exploring the potential of combining this formulation with other lightweight and sustainable materials holds great promise. Investigating the use of natural fibers or other recycled materials could lead to the development of next-generation automotive parts with even greater environmental benefits.

■ ASSOCIATED CONTENT

Supporting Information

The Supporting Information is available free of charge at https://pubs.acs.org/doi/10.1021/acsomega.4c02596.

Characterization of talc, graphene/talc hybrid, and GNP selected as reinforcing agents; photograph of mechanically recycled waste PP; the composition details of the prepared CopoPP compounds; injection parameters for production of B pillar interior part from the optimized compound formulation; structural FEA methodology and its boundary conditions; fractured surface SEM of the composites; structural analysis output and performance tests of the produced part; and environmental impact factors obtained from LCA analysis (PDF)

■ AUTHOR INFORMATION

Corresponding Author

Burcu Saner Okan − *Sabanci University Integrated Manufacturing Technologies Research and Application Center & Composite Technologies Center of Excellence, Pendik 34906 Istanbul, Turkey; Faculty of Engineering and Natural Sciences, Materials Science and Nanoengineering, Sabanci University, Tuzla 34956 Istanbul, Turkey;* orcid.org/0000-0002-5940-7345; Email: bsanerokan@sabanciuniv.edu

Authors

Havva Baskan-Bayrak − *Sabanci University Integrated Manufacturing Technologies Research and Application Center & Composite Technologies Center of Excellence, Pendik 34906 Istanbul, Turkey*

Ramisa Yahyapour − *Sabanci University Integrated Manufacturing Technologies Research and Application Center & Composite Technologies Center of Excellence, Pendik 34906 Istanbul, Turkey; Faculty of Engineering and Natural Sciences, Materials Science and Nanoengineering, Sabanci University, Tuzla 34956 Istanbul, Turkey;* orcid.org/0009-0001-0629-3620

Yavuz Emre Yagci − *Taysad Organize Sanayi Bolgesi (TOSB), Farplas Otomotiv A.S., Kocaeli 41420, Turkey*

Complete contact information is available at: https://pubs.acs.org/10.1021/acsomega.4c02596

Author Contributions

H.B.B.: data curation, formal analysis, investigation, methodology, writing-original draft; R. Y.: data curation, formal analysis, investigation, writing-original draft; Y.E.Y.: data curation, formal analysis, investigation, methodology, software, validation; B.S.O.: conceptualization, funding acquisition, project administration, resources, supervision, visualization, validation, review and editing. All authors have approved the final version of the manuscript.

Funding

This work was supported by The Scientific and Technological Research Council of Turkey (TUBITAK) 1003 project with the code 218M658.

Notes

The authors declare no competing financial interest.

■ ACKNOWLEDGMENTS

The authors thank Kuray Dericiler and Nargiz Aliyeva for conducting SEM characterizations.

■ REFERENCES

(1) Dikshit, V.; Goh, G. D.; Nagalingam, A. P.; Goh, G. L.; Yeong, W. Y. Recent Progress in 3D Printing of Fiber-Reinforced Composite and Nanocomposites. In *Fiber-Reinforced Nanocomposites: Fundamentals and Applications*; Elsevier, 2020.

(2) Gogoi, R.; Maurya, A. K.; Manik, G. A Review on Recent Development in Carbon Fiber Reinforced Polyolefin Composites. *Compos., Part C: Open Access* **2022**, *8* (January 2023), 100279.

(3) Almushaikeh, A. M.; Alaswad, S. O.; Alsuhybani, M. S.; AlOtaibi, B. M.; Alarifi, I. M.; Alqahtani, N. B.; Aldosari, S. M.; Alsaleh, S. S.; Haidyrah, A. S.; Alolyan, A. A.; Alshammari, B. A. Manufacturing of Carbon Fiber Reinforced Thermoplastics and Its Recovery of Carbon Fiber: A Review. *Polym. Test.* **2023**, *122* (March), 108029.

(4) Jagadeesh, P.; Puttegowda, M.; Rangappa, S. M.; Siengchin, S. Role of Polymer Composites in Railway Sector: An Overview. *Appl. Sci. Eng. Prog.* **2022**, *15* (2), 5745.

(5) Zirak, N.; Shirinbayan, M.; Deligant, M.; Tcharkhtchi, A. Toward Polymeric and Polymer Composites Impeller Fabrication. *Polymers* **2022**, *14* (1), 97.

(6) Dos Santos, R. S.; da Silveira, P. H. P. M.; Bastos, B. C.; do Nascimento da Conceição, M.; da Conceição Ribeiro, R. C.; Bastos, D. C. Development of Environmentally Ecofriendly Composites Based on Polypropylene/Bahia Beige Waste: Effect of Reinforcement

Content on Physical, Mechanical, Chemical, and Microstructural Properties. *Recent Prog. Mater.* **2023**, *5* (3), 27.
(7) Ghoshal, S.; Wang, P. H.; Gulgunje, P.; Verghese, N.; Kumar, S. High Impact Strength Polypropylene Containing Carbon Nanotubes. *Polymer* **2016**, *100*, 259−274.
(8) Várdai, R.; Schäffer, Á.; Ferdinánd, M.; Lummerstorfer, T.; Jerabek, M.; Gahleitner, M.; Faludi, G.; Móczó, J.; Pukánszky, B. Crystalline Structure and Reinforcement in Hybrid PP Composites. *J. Therm. Anal. Calorim.* **2022**, *147* (1), 145−154.
(9) Selvam, M. A. J.; Padmanabhan, S.; Kumar, M. L. Investigation of Mechanical Behavior of Hybrid Polymer Composite. *Mater. Today: Proc.* **2022**, *59*, 1256−1260.
(10) Harada, K.; Fujimori, A.; Xu, K.; Fujimori, A. Polypropylene-Based Nanocomposite with Improved Mechanical Properties: Effect of Cellulose Nanofiber and Polyrotaxane with Partial Miscibility. *Polym. Compos.* **2023**, *44* (5), 2977−2987.
(11) Ramesh, M.; Rajeshkumar, L. N.; Srinivasan, N.; Kumar, D. V.; Balaji, D. Influence of Filler Material on Properties of Fiber-Reinforced Polymer Composites: A Review. *E-Polymers* **2022**, *22*, 898−916.
(12) Agarwal, J.; Sahoo, S.; Mohanty, S.; Nayak, S. K. Progress of Novel Techniques for Lightweight Automobile Applications through Innovative Eco-Friendly Composite Materials: A Review. *J. Thermoplast. Compos. Mater.* **2020**, *33* (7), 978−1013.
(13) Jahani, Y. Dynamic Rheology, Mechanical Performance, Shrinkage, and Morphology of Chemically Coupled Talc-Filled Polypropylene. *J. Vinyl Addit. Technol.* **2010**, *16*, 70−77.
(14) Guerrica-Echevarría, G.; Eguiazábal, J. I.; Nazábal, J. Influence of Molding Conditions and Talc Content on the Properties of Polypropylene Composites. *Eur. Polym. J.* **1998**, *34* (8), 1213−1219.
(15) Castillo, L. A.; Barbosa, S. E. Influence of Processing and Particle Morphology on Final Properties of Polypropylene/Talc Nanocomposites. *Polym. Compos.* **2020**, *41* (8), 3170−3183.
(16) Tadele, D.; Roy, P.; Defersha, F.; Misra, M.; Mohanty, A. K. A Comparative Life-Cycle Assessment of Talc- and Biochar-Reinforced Composites for Lightweight Automotive Parts. *Clean Technol. Environ. Policy* **2020**, *22* (3), 639−649.
(17) Thariq, M.; Sultan, H. *Tribological Applications of Composite Materials*; Springer Singapore, 2021; .
(18) Shah, V.; Bhaliya, J.; Patel, G. M.; Deshmukh, K. Advances in Polymeric Nanocomposites for Automotive Applications: A Review. *Polym. Adv. Technol.* **2022**, *33* (10), 3023−3048.
(19) Saba, N.; Tahir, P. M.; Jawaid, M. A Review on Potentiality of Nano Filler/Natural Fiber Filled Polymer Hybrid Composites. *Polymers* **2014**, *6* (8), 2247−2273.
(20) Kuilla, T.; Bhadra, S.; Yao, D.; Kim, N. H.; Bose, S.; Lee, J. H. Recent Advances in Graphene Based Polymer Composites. *Prog. Polym. Sci.* **2010**, *35* (11), 1350−1375.
(21) Daniel, N.; Liu, H. Graphene Polymer Composites: Review on Fabrication Method, Properties and Future Perspectives. *Adv. Sci. Technol. Res. J.* **2021**, *15* (1), 37−49.
(22) El Achaby, M.; Arrakhiz, F. E.; Vaudreuil, S.; Qaiss, A.; Bousmina, M.; Fassi-Fehri, O. Mechanical, Thermal, and Rheological Properties of Graphene-Based Polypropylene Nanocomposites Prepared by Melt Mixing. *Polym. Polym. Compos.* **2012**, *33*, 733−744.
(23) Ferrari, A. C.; Bonaccorso, F.; Fal'ko, V.; Novoselov, K. S.; Roche, S.; Bøggild, P.; Borini, S.; Koppens, F. H. L.; Palermo, V.; Pugno, N.; et al. Science and Technology Roadmap for Graphene, Related Two-Dimensional Crystals, and Hybrid Systems. *Nanoscale* **2015**, *7* (11), 4598−4810.
(24) Rocha, M. C.; Alvarez Acevedo, N. I.; Futigami, J.; Jiménez, Y.; da Silva, A. L. N. Polypropylene Hybrid Composites for the Automotive Industry. In *International Conference on Composites Materials*, 2023.
(25) Liang, J. Z.; Du, Q. Melt Flow and Flexural Properties of Polypropylene Composites Reinforced with Graphene Nano-Platelets. *Int. Polym. Process.* **2018**, *33* (1), 35−41.
(26) Patra, S. C.; Swain, S.; Senapati, P.; Sahu, H.; Murmu, R.; Sutar, H. Polypropylene and Graphene Nanocomposites: Effects of Selected 2D-Nanofiller's Plate Sizes on Fundamental Physicochemical Properties. *Inventions* **2022**, *8* (1), 8.
(27) Sutar, H.; Mishra, B.; Senapati, P.; Murmu, R.; Sahu, D. Mechanical, Thermal, and Morphological Properties of Graphene Nanoplatelet-Reinforced Polypropylene Nanocomposites: Effects of Nanofiller Thickness. *J. Compos. Sci.* **2021**, *5*, 24.
(28) Zanjani, J. S. M.; Poudeh, L. H.; Ozunlu, B. G.; Yagci, Y. E.; Menceloglu, Y.; Saner Okan, B. Development of Waste Tire-Derived Graphene Reinforced Polypropylene Nanocomposites with Controlled Polymer Grade, Crystallization and Mechanical Characteristics via Melt-Mixing. *Polym. Int.* **2020**, *69* (9), 771−779.
(29) Kocanalı, A.; Baskan-Bayrak, H.; Menceloglu, Y.; Saner Okan, B. A Selective Upcycling Approach: Growing 2D and 3D Graphene Oxide Structures with Size-Controlled Talc Substrates from Waste Polypropylene with LCA Protocols. *J. Polym. Environ.* **2023**, *31* (9), 4052−4068.
(30) Yalcinkaya, E.; Baskan-bayrak, H.; Saner, B. Growing of 2D/3D Graphene Structures on Natural Substrates from Aromatic Plastic Wastes by Scalable Thermal-Based Upcycling Process with a Comparative CO 2 Footprint Analysis. *Sustainable Mater. Technol.* **2023**, *37* (August), No. e00687.
(31) Okan, B. S.; Menceloğlu, Y.; Ozunlu, B. G.; Yagci, Y. E. Graphene from Waste Tire by Recycling Technique for Cost-Effective and Light-Weight Automotive Plastic Part Production. *AIP Conf. Proc.* **2020**, *2205* (January), 020046.
(32) Gray, R. G.; Gottlieb, N. L. Hand flexor tenosynovitis in rheumatoid arthritis. *Arthritis Rheum.* **1977**, *20* (4), 1003−1008.
(33) Lapcik, L.; Jindrova, P.; Lapcikova, B.; Tamblyn, R.; Greenwood, R.; Rowson, N. Effect of the Talc Filler Content on the Mechanical Properties of Polypropylene Composites. *J. Appl. Polym. Sci.* **2008**, *110* (5), 2742−2747.
(34) Wang, K.; Bahlouli, N.; Addiego, F.; Ahzi, S.; Rémond, Y.; Ruch, D.; Muller, R. Effect of Talc Content on the Degradation of Re-Extruded Polypropylene/Talc Composites. *Polym. Degrad. Stab.* **2013**, *98* (7), 1275−1286.
(35) Ashenai Ghasemi, F.; Ghasemi, I.; Menbari, S.; Ayaz, M.; Ashori, A. Optimization of Mechanical Properties of Polypropylene/Talc/Graphene Composites Using Response Surface Methodology. *Polym. Test.* **2016**, *53*, 283−292.
(36) de Oliveira, C. I. R.; Rocha, M. C. G.; de Assis, J. T.; da Silva, A. L. N. Morphological, Mechanical, and Thermal Properties of PP/SEBS/Talc Composites. *J. Thermoplast. Compos. Mater.* **2022**, *35* (2), 281−299.
(37) Singh, A. K.; Chhetri, M. S.; Mishra, P. Toughness and Ductile Brittle Transition Temperature of Different Mineral Filler Reinforced TPOS Composites. *Sci. Temper* **2022**, *13* (2), 258−264.
(38) Zihlif, A. M.; Ragosta, G. Mechanical Properties of Talc-Polypropylene Composites. *Mater. Lett.* **1991**, *11* (10−12), 368−372.
(39) Ghanbari, A.; Behzadfar, E.; Arjmand, M. Properties of Talc Filled Reactor-Made Thermoplastic Polyolefin Composites. *J. Polym. Res.* **2019**, *26* (10), 241.
(40) Castillo, L. A.; Barbosa, S. E.; Capiati, N. J. Influence of Talc Morphology on the Mechanical Properties of Talc Filled Polypropylene. *J. Polym. Res.* **2013**, *20* (5), 152.
(41) Jun, Y. S.; Um, J. G.; Jiang, G.; Yu, A. A Study on the Effects of Graphene Nano-Platelets (GnPs) Sheet Sizes from a Few to Hundred Microns on the Thermal, Mechanical, and Electrical Properties of Polypropylene (PP)/GnPs Composites. *eXPRESS Polym. Lett.* **2018**, *12* (10), 885−897.
(42) Joshi, M.; Brahma, S.; Roy, A.; Wazed Ali, S. Nano-Calcium Carbonate Reinforced Polypropylene and Propylene-Ethylene Copolymer Nanocomposites: Tensile vs. Impact Behavior. *Fibers Polym.* **2017**, *18* (11), 2161−2169.
(43) Papageorgiou, D. G.; Kinloch, I. A.; Young, R. J. Mechanical Properties of Graphene and Graphene-Based Nanocomposites. *Prog. Mater. Sci.* **2017**, *90*, 75−127.
(44) Ezenkwa, O. E.; Hassan, A.; Samsudin, S. A. Comparison of Mechanical Properties and Thermal Stability of Graphene-Based Materials and Halloysite Nanotubes Reinforced Maleated Polymer

https://doi.org/10.1021/acsomega.4c02596
ACS Omega 2024, 9, 34530−34543

Compatibilized Polypropylene Nanocomposites. *Polym. Compos.* **2022**, *43* (3), 1852−1863.
(45) Landel, R. F.; Nielsen, L. E. *Mechanical Properties of Polymers and Composites*; CRC Press, 1993.
(46) Tsue, F.; Takahashi, Y.; Shimizu, H. Reinforcing Effect of Glass-Fiber-Reinforced Composite on Flexural Strength at the Proportional Limit of Denture Base Resin. *Acta Odontol. Scand.* **2007**, *65* (3), 141−148.
(47) Li, S.; Chen, L.; Gui, X.; He, D.; Hu, J.; Huang, Z.; Lin, S.; Tu, Y.; Dong, Y. Molecular Dynamics Simulation for Thiolated Poly-(Ethylene Glycol) at Low-Temperature Based on the Density Functional Tight-Binding Method. *Adv. Theory Simul.* **2022**, *5* (12), 2200281.
(48) Caicedo, C.; Vázquez-Arce, A.; Ossa, O. H.; De La Cruz, H.; Maciel-Cerda, A. Physicomechanical Behavior of Composites of Polypropylene, and Mineral Fillers with Different Process Cycles. *DYNA* **2018**, *85* (207), 260−268.
(49) Sarturato, A. C. P.; Dos Anjos, E. G. R.; Marini, J.; Morgado, G. F. D. M.; Baldan, M. R.; Passador, F. R. Polypropylene/Talc/Graphene Nanoplates (GNP) Hybrid Composites: Effect of GNP Content on the Thermal, Rheological, Mechanical, and Electrical Properties. *J. Appl. Polym. Sci.* **2023**, *140* (12), 1−13.
(50) Selvakumar, V.; Manoharan, N. Thermal Properties of Polypropylene/Montmorillonite Nanocomposites. *Indian J. Sci. Technol.* **2014**, *7* (7), 136−139.
(51) Jabarin, S. A.; Majdzadeh-Ardakani, K.; Lofgren, E. A. Crystallization and Melting Behavior in Polymer Blends. *Encycl. Polym. Blends* **2016**, *1*, 135−190.
(52) Qiu, Z.; Yan, C.; Lu, J.; Yang, W. Miscible Crystalline/Crystalline Polymer Blends of Poly(Vinylidene Fluoride) and Poly (Butylene Succinate-Co-Butylene Adipate): Spherulitic Morphologies and Crystallization Kinetics. *Macromolecules* **2007**, *40* (14), 5047−5053.
(53) Cho, K.; Li, F.; Choi, J. Crystallization and Melting Behavior of Polypropylene and Maleated Polypropylene Blends. *Polymer* **1999**, *40* (7), 1719−1729.
(54) Cetiner, B.; Sahin Dundar, G.; Yusufoglu, Y.; Saner Okan, B. Sustainable Engineered Design and Scalable Manufacturing of Upcycled Graphene Reinforced Polylactic Acid/Polyurethane Blend Composites Having Shape Memory Behavior. *Polymers* **2023**, *15* (5), 1085.
(55) Nekhlaoui, S.; Essabir, H.; Kunal, D.; Sonakshi, M.; Bensalah, M.; Bouhfid, R.; Qaiss, A. Comparative Study for the Talc and Two Kinds of Moroccan Clay as Reinforcements in Polypropylene-SEBS-g-MA Matrix. *Polym. Compos.* **2015**, *36*, 675−684.
(56) Fosse, C.; Bourdet, A.; Ernault, E.; Esposito, A.; Delpouve, N.; Delbreilh, L.; Thiyagarajan, S.; Knoop, R. J. I.; Dargent, E. Determination of the Equilibrium Enthalpy of Melting of Two-Phase Semi-Crystalline Polymers by Fast Scanning Calorimetry. *Thermochim. Acta* **2019**, *677* (November2018), 67−78.
(57) Altay, L.; Atagur, M.; Sever, K.; Sen, I.; Uysalman, T.; Seki, Y.; Sarikanat, M. Synergistic Effects of Graphene Nanoplatelets in Thermally Conductive Synthetic Graphite Filled Polypropylene Composite. *Polym. Compos.* **2019**, *40* (1), 277−287.
(58) Pandey, A. K.; Pal, T.; Sharma, R.; Kar, K. K. Study of Matrix-Filler Interaction through Correlations between Structural and Viscoelastic Properties of Carbonous-Filler/Polymer-Matrix Composites. *J. Appl. Polym. Sci.* **2020**, *137* (27), 48660.
(59) Papageorgiou, D. G.; Terzopoulou, Z.; Fina, A.; Cuttica, F.; Papageorgiou, G. Z.; Bikiaris, D. N.; Chrissafis, K.; Young, R. J.; Kinloch, I. A. Enhanced Thermal and Fire Retardancy Properties of Polypropylene Reinforced with a Hybrid Graphene/Glass-Fibre Filler. *Compos. Sci. Technol.* **2018**, *156*, 95−102.
(60) Tajvidi, M. Static and Dynamic Mechanical Properties of a Kenaf Fiber-Wood Flour/Polypropylene Hybrid Composite. *J. Appl. Polym. Sci.* **2005**, *98* (2), 665−672.
(61) Papageorgiou, D. G.; Kinloch, I. A.; Young, R. J. Hybrid Multifunctional Graphene/Glass-Fibre Polypropylene Composites. *Compos. Sci. Technol.* **2016**, *137*, 44−51.
(62) Le, M. T.; Huang, S. C. Thermal and Mechanical Behavior of Hybrid Polymer Nanocomposite Reinforced with Graphene Nanoplatelets. *Materials* **2015**, *8* (8), 5526−5536.
(63) Maiti, S. N.; Sharma, K. K. Studies on Polypropylene Composites Filled with Talc Particles. *J. Mater. Sci.* **1992**, *27* (17), 4605−4613.
(64) Liao, J.; Brosse, N.; Pizzi, A.; Hoppe, S.; Xi, X.; Zhou, X. Polypropylene Blend with Polyphenols through Dynamic Vulcanization: Mechanical, Rheological, Crystalline, Thermal, and UV Protective Property. *Polymers* **2019**, *11* (7), 1108.
(65) Díez-Gutiérrez, S.; Rodríguez-Pérez, M. A.; De Saja, J. A.; Velasco, J. I. Dynamic Mechanical Analysis of Injection-Moulded Discs of Polypropylene and Untreated and Silane-Treated Talc-Filled Polypropylene Composites. *Polymer* **1999**, *40* (19), 5345−5353.
(66) Melo de Lima, L. R.; Dias, A. C.; Trindade, T.; Oliveira, J. M. A Comparative Life Cycle Assessment of Graphene Nanoplatelets- and Glass Fibre-Reinforced Poly(Propylene) Composites for Automotive Applications. *Sci. Total Environ.* **2023**, *871* (February), 162140.

https://doi.org/10.1021/acsomega.4c02596
ACS Omega 2024, 9, 34530−34543